ISSN 1063-7834, Physics of the Solid State, 2019, Vol. 61, No. 3, pp. 332–338. © Pleiades Publishing, Ltd., 2019.
Russian Text © E.A. Gan'shina, L.L. Golik, Z.E. Kun'kova, G.S. Zykov, Yu.V. Markin, Yu.A. Danilov, B.N. Zvonkov, 2019, published in Fizika Tverdogo Tela, 2019, Vol. 61, No. 3, pp. 465–471.

MAGNETISM

Phase Separation in (Ga,Mn)As Layers Obtained by Ion Implantation and Subsequent Laser Annealing

E. A. Gan'shina[a,*], L. L. Golik[b], Z. E. Kun'kova[b], G. S. Zykov[a], Yu. V. Markin[b], Yu. A. Danilov[c], and B. N. Zvonkov[c]

[a] *Lomonosov Moscow State University, Moscow, 119991 Russia*

[b] *Fryazino Branch of Kotelnikov Institute of Radioengineering and Electronics, Russian Academy of Science, Fryazino, 141190 Russia*

[c] *Lobachevsky State University of Nizhny Novgorod, Nizhny Novgorod, 603022 Russia*

**e-mail: eagan@mail.ru*

Received October 2, 2018

Abstract—In this paper, we present the results of studies of the spectral, temperature, and field dependences of the transversal Kerr effect in $Ga_{1-x}Mn_xAs$ ($x = 0.0066–0.033$) layers produced by ion implantation and subsequent pulsed laser annealing. The complicated nonmonotonous nature of the temperature dependences of the transversal Kerr effect and its dependence on the measurement range indicate a magnetic inhomogeneity of the layers. The reasons for the inhomogeneity can be the Gaussian distribution of Mn over the thickness of the layers and the electron phase separation in them. The appearance of new features in the spectra of the transversal Kerr effect is explained by the presence in the doped semiconductor matrix of nanoregions with a higher carrier concentration and a higher Curie temperature and a shift of the Fermi level into the valence band leading to an increase in the energy of optical transitions.

DOI: 10.1134/S1063783419030119

1. INTRODUCTION

Ga(In)As-based systems doped with Mn belong to dilute magnetic semiconductors (DMS) and are considered as promising materials for various spintronic and magneto-photonic devices [1–3]. Despite its nearly 20-year history of research, (Ga,Mn)As remains one of the most studied and, at the same time, one of the most controversial objects in condensed matter physics [1–4]. This is due to several major reasons. Firstly, replacing Ga, Mn ions act as acceptors and supply holes that are involved in the ferromagnetic ordering of localized moments of Mn. Secondly, the presence of randomly distributed acceptors leads to substantial disorder and fluctuations in the local electron density of carriers, i.e., to electronic phase separation [4]. This electronic phase separation can lead to a metal-insulator transition (MIT) in the region of hole densities corresponding to the ferromagnetic phase and the formation of inclusions from nanoscale metallic ferromagnetic regions (enriched with holes) in an insulating nonferromagnetic matrix (depleted in holes). The presence of carrier-mediated exchange interactions and the Anderson–Mott quantum localization leads to unique properties that have not yet been theoretically described.

Electron phase separation in (Ga,Mn)As was experimentally observed in layers obtained by low-temperature molecular beam epitaxy (LT-MBE) [5–7] and was theoretically explained taking into account nuclear quantum effects [8]. However, there are always compensating defects in these layers: interstitial Mn and antisite As replacing Ga in the lattice sites. The types of structural and point defects and, therefore, the concentration of free carriers, the position of the Fermi level, and the nature of possible phase inhomogeneities depend on the growth technology.

Contrary to the films formed by LT-MBE, in the (Ga,Mn)As layers produced by ion implantation with subsequent pulsed laser annealing (PLA), there are practically no defects associated with interstitial Mn and antisite As [9, 10]. These samples provide a unique opportunity to study the effects of localization and electron phase separation near the metal–insulator transition, where these effects should appear most clearly.

Methods of magneto-optical (MO) spectroscopy [11–14] are widely used to study the DMS electronic spectrum and to elucidate the mechanism of ferromagnetic exchange. MO properties are sensitive both to long-range magnetic order and to the appearance of short-range order. Therefore, the presence of magnetic phase inhomogeneities should manifest itself in the appearance of additional features in the spectral and temperature dependences of the MO response.

Table 1. Conditions for preparation and parameters of the $Ga_{1-x}Mn_xAs$ samples 1–5

Sample no.	1	2	3	4	5
Mn concentration, x (%), SRIM modeling x_{peak}	≈1	≈1.5	≈2	≈4	≈6
by SIMS (%)	0.66	0.87	1.2	1.8	~3.3*
Radiation density (cm^{-2}) of XeCl excimer laser, $\lambda = 308$ nm, $\tau = 28$ ns	1×10^{15}	1.5×10^{15}	2×10^{15}	8×10^{15}	1×10^{16}
Annealing energy (J/cm^2)	0.3	0.3	0.3	0.3	0.3
$T_C(T_\sigma)$ (K) from measuring $M(T)$	7.5	17	31	60	60
M_s (emu/cm^3)	2.8	5.0	7.75	14.0	26.7**
Layer thickness (nm)	60	60	60	60	60

* Since SIMS measurements for sample 5 have not been performed, the Mn concentration, x, in sample 5 has been estimated based on the saturation magnetization value.
** Under the assumption that each implanted Mn ion replaces the Ga ion and produces one carrier (hole). $M_s = xN_0m_{Mn}$, $N_0 = 2.2 \times 10^{22}$ cm^{-3}, and $m_{Mn} = 4$ μB.

When comparing the MO and transport properties of a series of GaMnAs samples produced by laser ablation, the behavior of low-temperature MO response in them was shown to be due to the presence of ferromagnetic (FM) clusters (Ga,Mn)As in a paramagnetic (PM) semiconductor matrix [15]. At the same time, in relatively low-doped (Ga,Mn)As samples produced by ion implantation and PLA, the ferromagnetic order was established to evolve from the PM phase to the FM phase through the formation of superparamagnetic (SPM) clusters [16]. The MO spectra of the same samples differ from the MO spectra of the layers produced by LT-MBE and laser ablation, but can be explained based on the valence-band model of ferromagnetism under the assumption of electron phase separation in them [17].

In this paper, we present additional experimental data confirming the phase inhomogeneity of relatively low-doped (Ga,Mn)As layers produced by ion implantation followed by laser annealing.

2. SAMPLES AND RESEARCH METHODS

The studied $Ga_{1-x}Mn_xAs$ layers on GaAs(001) substrates were prepared by ion implantation at room temperature at the Ion Beam Center, Helmholtz-Zentrum Dresden-Rossendorf (Germany). Mn ions were implanted into undoped GaAs(001) wafers at the energy of 100 keV and incidence angle of 7° to prevent ion channeling. According to the SRIM modeling with allowance for the radiation density of 1×10^{15}–1×10^{16} cm^{-2}, the expected concentration of Mn (x) should be in the range from 0.01 to 0.06. A coherent XeCl excimer laser with a wavelength of 308 nm and a pulse duration of 28 ns was used to anneal the implanted GaAs layer. The uniform profile of the laser beam was 5×5 mm^2. The optimized annealing energy was 0.3 J/cm^2. After laser annealing, the number of Mn atoms introduced into the GaAs layer differs from the planned value since a part of the implanted Mn atoms diffuses to the surface during recrystallization. To remove the Mn-rich surface layer, the sample surface was etched in a concentrated hydrochloric acid. In so doing, the majority of implanted Mn atoms remain inside the GaAs matrix. The Mn concentration profiles were determined by secondary ion mass spectrometry (SIMS). The distribution of Mn is approximately Gaussian. Since the measured Curie temperature is determined by the peak Mn concentration in the distribution, the Mn concentration was determined as an average value within the coherence length (~5 nm) in the region around the maximum.

More information on obtaining the samples has been published elsewhere [18, 19]. The results of SIMS studies, transmission electron microscopy (TEM), and also magnetometric and electrical measurements are presented in [16].

The sample preparation conditions, the planned and SIMS-determined x-values, spontaneous magnetization (M_S) magnitudes and the values of the sample thickness, as well as the Curie temperature (T_C) values obtained by magnetometry, are given in Table 1.

Magneto-optical properties were studied in the geometry of the transversal Kerr effect (TKE), which consists in changing the intensity of p-polarized light reflected by a sample when magnetized in a magnetic field parallel to the sample surface and perpendicular to the plane of light incidence. The TKE value, $\delta = [I(H) - I(-H)]/2I(0)$, where $I(H)$ and $I(0)$ are, respectively, the intensities of reflected light in the presence and absence of a magnetic field, is measured by the dynamic method at modulation of the magnetic field.

The TKE spectra, $\delta(E)$, were recorded in the energy range of $E = 0.5$–4.0 eV in the magnetic fields up to 3 kOe. The studied temperature range is $T = 15$–295 K, and the equipment sensitivity to changes in the light intensity is ~10^{-5} [20]. The value of effective

Curie temperature was determined based on the temperature dependences of TKE by extrapolation to zero of the sharp fall section in the $\delta(T)$ curve measured when heating.

In the dynamic method of measurement, the TKE value linearly depends on magnetization, and measuring the temperature, $\delta(T)$, and field, $\delta(H)$, TKE dependences at a fixed energy of the incident light allows characterizing the magnetic state of a sample. For homogeneous samples, the temperature and field dependences of the reduced $\delta(T)/\delta_{max}$ and $\delta(H)/\delta(H_{max})$ values should not depend on the incident light energy. However, in the case of phase separation and the presence of several magnetic phases with different Curie temperatures (T_C), exchange splitting values and the Fermi level position, the $\delta(T)/\delta_{max}$ and $\delta(H)/\delta(H_{max})$ dependences should depend on the measurement range.

3. RESULTS AND DISCUSSION

At room temperature, the TKE signal from the samples under study is not recorded, i.e., the possible high-temperature ferromagnetic MnAs phase is absent in them. At low temperatures, there is a strong MO response from all samples. The TKE spectra of samples 1–5 in the range of 0.5–4.0 eV are given in our recent study [17].

The TKE spectra are shown in Fig. 1 for the range of $E = 1.0$–4.0 eV, which includes the edge and intrinsic absorption region of GaAs. The TKE spectra of samples 1–4 are seen to be similar. In the range of $E <$ 2.5 eV, the spectra contain a negative polarity band with two local minima near the energies of the transitions E_0 and $E_0 + \Delta_0$ (≈1.5 and 1.8 eV) in GaAs. As the Mn concentration increases, these features monotonously increase, and their weak blue shift is observed. In the spectrum of sample 5, the shape of the negative band changes along with a significant increase in TKE. Instead of two minima in the spectrum of sample 5, there is one negative peak around 1.6 eV. In the spectra of all the samples, there is a negative polarity band ($E_{max} \approx 3.05$ eV) in the region of the E_1, $E_1 + \Delta_1$ transitions (at the L-point) in GaAs. With increasing the Mn concentration, this band increases without changing the shape. A magnified image of this band is shown in the inset in Fig. 1.

Most often, magnetic circular dichroism (MCD) spectroscopy is used to study the electronic structure of $(A^3,Mn)B^5$, since the MCD signal amplifies near the critical points of the Brillouin zone of the original semiconductor. We calculated the MCD spectra of samples 1–5 [17]. All the features that can be seen in Fig. 1 are present in the calculated spectra at close energies. The difference between the TKE and MCD spectra consists in the change in the polarity of the band near 3.05 eV to the positive one and in an increase in its relative intensity. The presence of this band in the MCD spectra is an evidence of the preservation of the GaAs crystal structure and intrinsic ferromagnetism of (Ga,Mn)As, since the introduction of high Mn concentrations, which noticeably changes the energy and intensity of the transitions near the Γ point, has a little effect on the transitions near the L point remote from the Brillouin zone center.

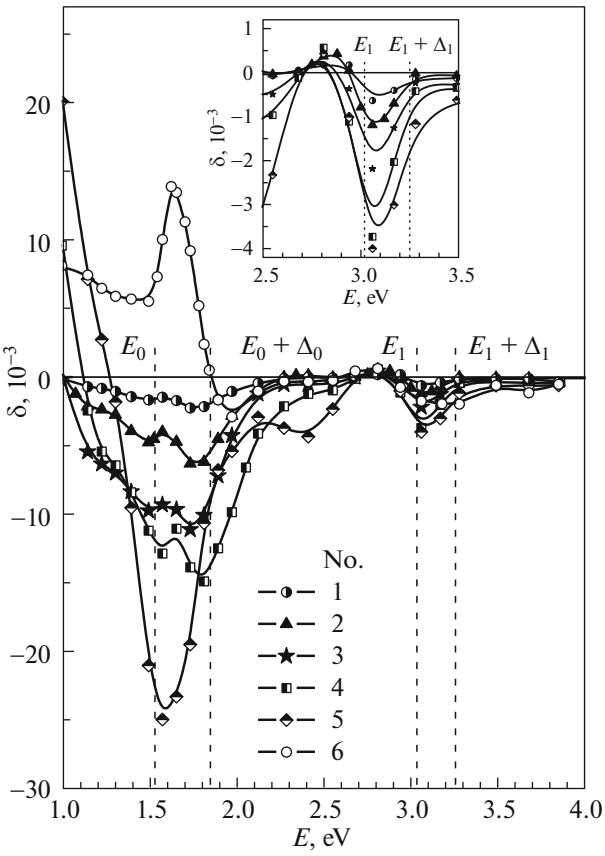

Fig. 1. TKE spectra of samples 1–5 at $T = 17$ K and the incidence angle of $\varphi = 68°$, as well as the spectrum of reference sample 6 ($T = 20$ K, $\varphi = 67°$). Dashed lines show energies of the E_0, $E_0 + \Delta_0$, E_1 and $E_1 + \Delta_1$ transitions at the Γ and L critical points of GaAs at $T = 22$ K [21]. (The inset shows an enlarged image of the TKE band associated with the transitions near the L point in GaAs.)

The MCD spectra of our samples 1–5 with the wide negative band in the region of $1.0 \le E \le 2.1$ eV (in the region of contributions from the E_0 and $E_0 + \Delta_0$ transitions) differ from the published spectra [12, 22–24]. We associated this band with the superposition of contributions from regions with different concentrations of Mn and/or holes [17]. The presence of phase inhomogeneities in the studied samples should also manifest itself in the temperature and field dependences of TKE.

Figure 2 shows the magnetic field dependences of reduced TKE, $\delta(H)/\delta(H_{max})$, for samples 1–4 at $T =$ 16 K. The linear $\delta(H)/\delta(H_{max})$ dependence of sample

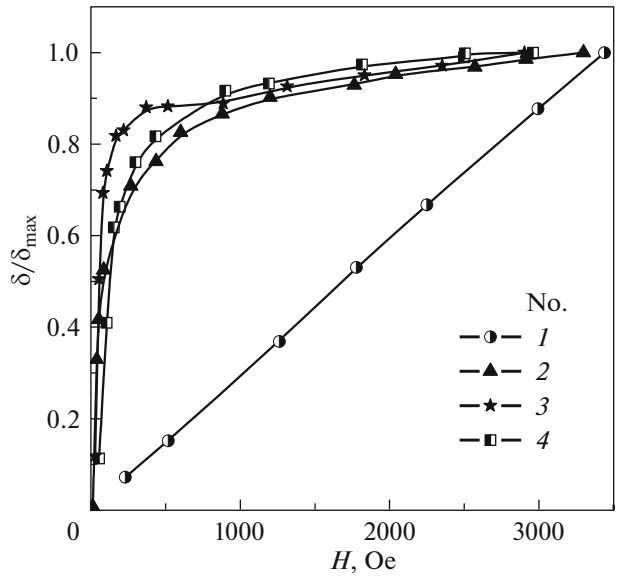

Fig. 2. Dependences of reduced value $\delta(H)/\delta(H_{max})$ on magnetic field for samples 1–4. $T = 16$ K. E, eV: (*1* and *2*) 1.73 and (*3* and *4*) 1.89. (To exclude overlap of the curves, $\delta(H)/\delta(H_{max})$ dependence for sample 5 is not shown).

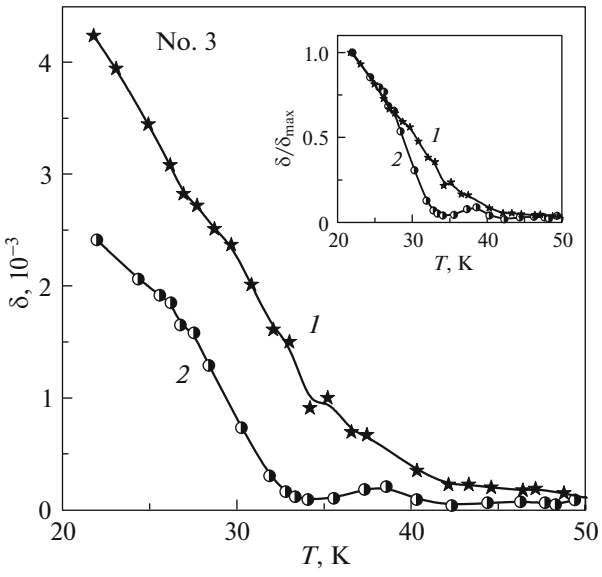

Fig. 3. TKE temperature dependences for sample 3 at $E = 1.57$ eV and two amplitudes of the magnetic field, H, Oe: (*1*) 1300 and (*2*) 100. Inset: $\delta(T)$ dependences normalized to the maximal value.

1 indicates the absence of a ferromagnetic phase at the measurement temperature and agrees with the data [16], according to which superparamagnetic granules with a size of 8–20 nm are contained in the paramagnetic matrix of the sample with $x = 0.0066$, ferromagnetic coupling in which occurs at $T \leq 7$ K.

The $\delta(H)/\delta(H_{max})$ curves of samples 2–5 demonstrate the presence of a ferromagnetic phase in them. At the same time, a paramagnetic component, whose slope and relative contribution decrease with increasing x, is observed in the fields of $H > 1000$ Oe.

The temperature dependences, $\delta(T)$, for samples 3–5 were measured near the extremes in the TKE spectra. Figure 3 illustrates changes in the TKE temperature dependence of sample 3 measured at $E = 1.57$ eV when decreasing the magnetic field amplitude from 1300 to 100 Oe. The decrease in H value leads to attenuation of the TKE signal, and in the inset in Fig. 3, the dependences $\delta(T)/\delta_{max}$ are shown to highlight qualitative changes in the $\delta(T)$ curves. The estimation of the effective Curie temperature using curves *1* produces the value of ≈40 K. At the same time, according to curves *2*, regions with $T_C \approx 32$ K (main contribution with T_C close to magnetometry data) and $T_C \approx 42$ K (weak contribution) contribute to the TKE signal. Distinction between curves *1* and *2* is apparently due to the ordering in the sufficiently strong measuring magnetic field of nanoscale ferromagnetic regions arising in the sample at temperatures slightly above T_C. The measurements in the weak field also revealed the contribution from local regions with the higher T_C value, i.e., they confirmed the magnetic inhomogeneity of sample 3.

Figures 4–6 show the TKE temperature dependences measured for samples 4 and 5, in which the Mn and holes concentration exceeds the boundary value ($x = 1.4\%$) of the formation of "global" ferromagnetism in the $Ga_{1-x}Mn_xAs$ layers obtained by the same method [16]. The temperature dependences, $\delta(T)/\delta_{max}$, for sample 4 normalized to maximum and measured at several energies and two magnetic field values are shown in Figs. 4a and 4b. As can be seen in the figures, the decrease in the magnetic field from 1500 to 95 Oe leads to a change in the shape of the $\delta(T)$ curves. At $T \leq 50$ K, the features most pronounced when measured in the small field and consisting in the replacement of the TKE increase by the decrease at cooling, are observed for the all curves.

As noted above, in a uniform ferromagnetic the TKE signal is proportional to the magnetization, and the $\delta(T)$ dependence reproduces the monotonic growth at decreasing T. If the electronic and/or magnetic structure of a sample is inhomogeneous, regions with differing characteristics can make contributions with opposite polarities to the total TKE spectrum. The competition of these contributions will affect the nature of the $\delta(T)$ dependence, and with comparable contributions the total signal decrease become possible. For the energies of 1.54, 1.73, and 3.06 eV, at which the $\delta(T)$ dependences have been measured, the polarity of the TKE signals is negative (Fig. 1), and the decrease in the signal at $T < 40$ K indicates the presence of a positive contribution and its growth during cooling. The presence in the spectrum of the contri-

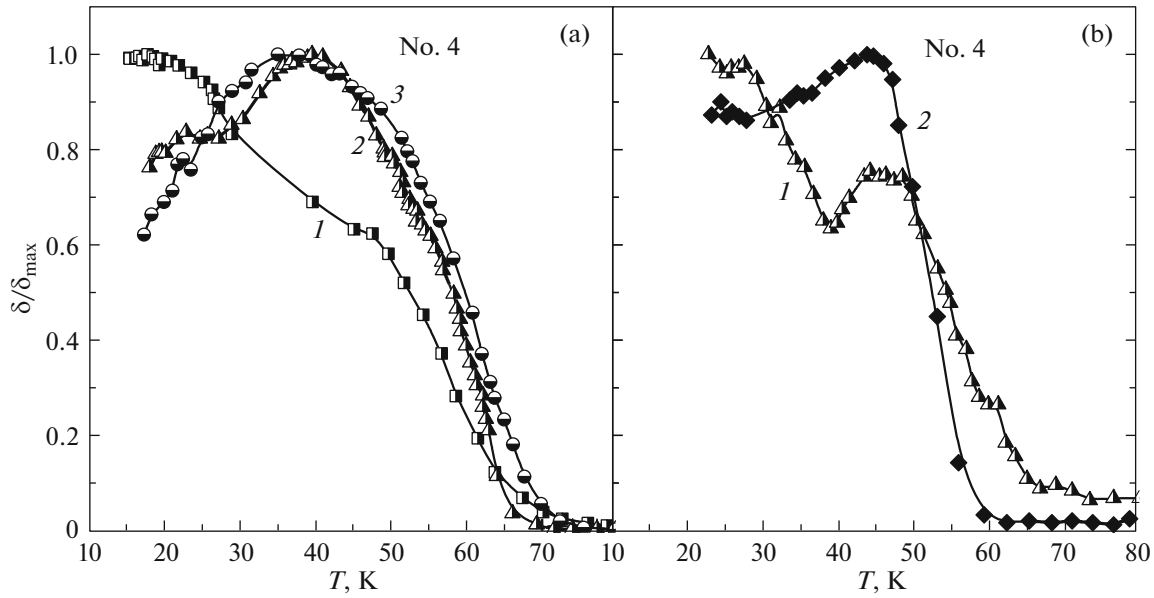

Fig. 4. $\delta(T)/\delta_{max}$ dependences for sample 4. (a) E, eV: (*1* and *2*) 1.54, (*3*) 1.73; H, Oe: (*1*) 1500, (*2* and *3*) 95. (b) $E = 3.06$ eV, H, Oe: (*1*) 2500 and (*2*) 95.

bution of positive polarity was detected when measuring in the region of weak signals. Figure 5 displays the $\delta(T)$ curve measured at $E = 2.41$ eV, which shows the appearance of a positive signal at approximately 70 K and the change in its polarity below 50 K.

Note that the decrease in the TKE signal with decreasing T depends on the measurement range. At $E = 1.73$ eV, the maximal absolute and relative (~40%) decrease in TKE is observed. The relative decrease in TKE at E = 1.54 and 3.06 eV is ~20% and 10%, respectively—see Figs. 4a and 4b. Therefore, the positive TKE contribution cannot be explained only by the monotonically falling "tail" of the impurity band, which has been observed in [17]. Metallic ferromagnetic inclusions with a higher T_C, as well as areas with a lower holes concentration and lower T_C value, whose positive TKE signal is associated with the $E_0 + \Delta_0$ transition, can be the sources of the signals with positive polarity.

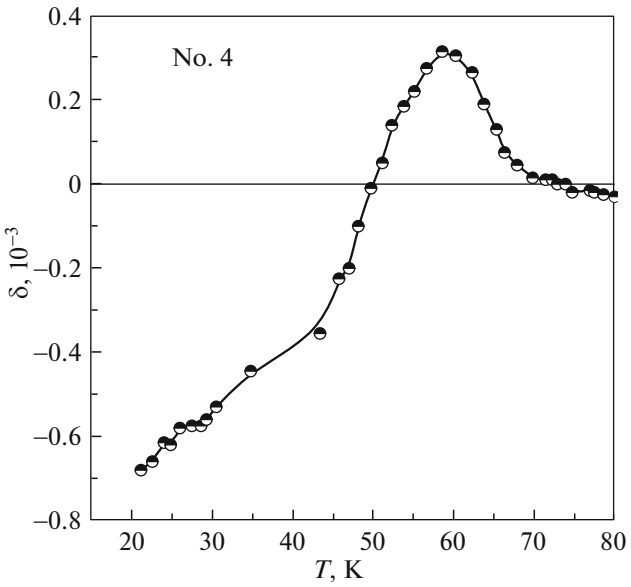

Fig. 5. $\delta(T)$ dependence for sample 4 at $E = 2.41$ eV and $H = 150$ Oe.

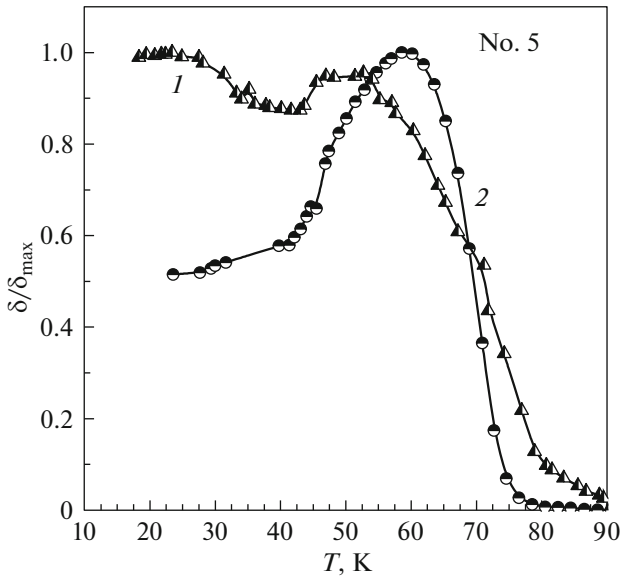

Fig. 6. Normalized $\delta(T)/\delta_{max}$ dependences for sample 5. $E = 1.73$ eV; H, Oe: (*1*) 1600 and (*2*) 90.

The estimation of effective T_C from the curves measured in the small field gives values of ≈67 K (E = 1.54 and 1.73 eV) and ≈70 K (E = 2.41 eV). Using the curve measured near the L point (E = 3.06 eV), the T_C value of ≈60 K, which coincides with the magnetometry data, was obtained. Comparison between the TKE temperature dependences and magnetic measurements data leads to the conclusion that the ferromagnetic phase with $T_C \approx 60$ K prevails in sample 4. However, along with this phase, there are ferromagnetic inclusions with the higher Curie temperature. It is possible that the detection of these inclusions contribution when measuring TKE is related to their localization in the near-surface region owing to migration of a part of implanted Mn ions to the surface during recrystallization after laser annealing. The presence in the sample of lower temperature regions, whose contribution to the total TKE signal is not spectrally resolved, is not excluded too.

Figure 6 shows the normalized $\delta(T)/\delta_{max}$ dependences of sample 5 ($x \sim 3.3\%$) measured at E = 1.73 eV in the strong (1600 Oe) and weak (90 Oe) magnetic fields. In the strong field, there is a slight drop in TKE at 45 K > T > 30 K. In the weak field, the signal decreases by about 50% when cooled from 60 to 20 K. The estimation of the effective Curie temperature of sample 5 from curve *2* gives $T_C \approx 75$ K, which exceeds the data of magnetic measurements.

Temperature dependences, $\delta(T)$, at fixed energies were also measured for GaMnAs sample 6 produced by laser ablation, whose spectrum is shown in Fig. 1. The study of magneto-optical, electrical, and magnetic properties of samples from the same growth series has shown that sample 6 consists of a weakly doped paramagnetic matrix and local (Ga,Mn)As ferromagnetic regions with $T_C \approx 80$ K [15]. The $\delta(T)$ measurements near extremes in the TKE spectrum (E = 1.63, 1.97, and 3.17 eV) showed a monotonic increase in the $|\delta|$ value during cooling and the coincidence of the normalized curves within the measurement error. These data indicate that the TKE spectrum is formed by regions with close magnetic characteristics. The monotonic rise of $|\delta|$ and coincidence of the normalized dependences, $\delta(T)/\delta_{max}$, were also obtained when measuring $\delta(T)$ in different parts of the spectrum of a metal ferromagnetic (Ga,Mn)As sample (x = 6% and $T_C \approx 130$ K) grown by LT-MBE. The nonmonotonic character of the TKE temperature dependences of the $Ga_{1-x}Mn_xAs$ layers produced by ion implantation and laser annealing indicates a magnetic inhomogeneity of the layers in the larger range of Mn concentrations than it follows from the magnetic measurements [16].

Taking into account the inhomogeneity of the samples, the negative band in the TKE (and MCD) spectra of samples 1–4 can be associated with the superposition of contributions from the mesoscopic regions differing by the Curie temperature, hole concentration, Fermi level position, and transitions energy near the Γ point. These inhomogeneities are due to electron phase separation, the inhomogeneous (Gaussian) distribution of Mn ions over the sample thickness, and possibly an increased Mn concentration in the near-surface layer. The first extremum (about 1.5 eV) is associated with the transitions from the filled or almost filled valence band to the conduction band in the regions with a low hole concentration. The MCD spectra of these regions should also contain a less intense band of positive polarity near 1.8 eV associated with the transitions from the "split-off" valence band. However, there is the band of opposite polarity in the MCD spectra of our samples. Transitions in the regions with a higher hole concentration and a marked Burstein–Moss shift are the possible cause of the second negative band. The presence of one negative peak (about 1.59 eV) in the spectra of sample 5 can be caused by the superposition of the negative contributions from dissimilar regions due to the convergence of their characteristics at increasing the Mn concentration.

4. CONCLUSIONS

Measured at various photon energies, the temperature dependences, $\delta(T)$, of the ferromagnetic $Ga_{1-x}Mn_xAs$ (x = 0.012–0.033) layers fabricated by ion implantation and subsequent laser annealing reveal their magnetic inhomogeneity. The reasons for the inhomogeneity can be the Gaussian distribution of Mn over the layers thickness and electron phase separation in them. The appearance of new (previously unobservable) features in the TKE and MCD spectra can be associated with the presence in the doped semiconductor matrix of the regions with a higher carrier concentration, higher T_C, and shift of the Fermi level into the valence band.

ACKNOWLEDGMENTS

The authors are grateful to Dr. Zhou (Institute of Ion Physics and Materials Research, Dresden–Rossendorf, Germany) for providing the $Ga_{1-x}Mn_xAs$ samples for the study.

The work was supported by the Ministry of Education and Science of the Russian Federation, project no. 8.1751.2017/PCh and the Russian Foundation for Basic Research, project no. 16-07-01102_a.

REFERENCES

1. T. Dietl and H. Ohno, Rev. Mod. Phys. **86**, 187 (2014).
2. T. Jungwirth, J. Wunderlich, V. Novak, K. Olejnık, B. L. Gallagher, R. P. Campion, K. W. Edmonds, A. W. Rushforth, A. J. Ferguson, and P. Nemec, Rev. Mod. Phys. **86**, 855 (2014).
3. M. Tanaka, S. Ohya, and P. Nam Hai, Appl. Phys. Rev. **1**, 011102 (2014).

4. T. Dietl, K. Sato, T. Fukushima, A. Bonanni, M. Jamet, A. Barski, S. Kuroda, M. Tanaka, Pham Nam Hai, and H. Katayama-Yoshida, Rev. Mod. Phys. **87**, 1311 (2015).
5. A. Richardella, P. Roushan, S. Mack, B. Zhou, D. A. Huse, D. D. Awschalom, and A. Yazdani, Science (Washington, DC, U. S.) **327**, 665 (2010).
6. M. Sawicki, D. Chiba, A. Korbecka, Y. Nishitani, J. A. Majewski, F. Matsukura, T. Dietl, and H. Ohno, Nat. Phys. **6**, 22 (2010).
7. L. Gluba, O. Yastrubchak, J. Z. Domagala, R. Jakiela, T. Andrearczyk, J. Żuk, T. Wosinski, J. Sadowski, and M. Sawicki, Phys. Rev. B **97**, 115201 (2018).
8. S. Bae and H. Raebiger, Phys. Rev. B **94**, 241115(R) (2016).
9. S. Zhou, J. Phys. D **48**, 263001 (2015).
10. M. Khalid, E. Weschke, W. Skorupa, M. Helm, and S. Zhou, Phys. Rev. B **89**, R121301 (2014).
11. K. Ando, Springer Ser. Solid State Sci. **128**, 211 (2000).
12. K. Ando, H. Saito, K. C. Agarwal, M. C. Debnath, and V. Zayets, Phys. Rev. Lett. **100**, 067204 (2008).
13. E. A. Gan'shina, L. L. Golik, V. I. Kovalev, Z. E. Kun'kova, A. G. Temiryazev, Yu. Danilov, O. V. Vikhrova, B. N. Zvonkov, A. D. Rubacheva, P. N. Tcherbak, A. N. Vinogradov, and O. M. Zhigalina, J. Phys.: Condens. Matter **22**, 396002 (2010).
14. C. Sun, J. Kono, Y.-H. Cho, A. K. Wojcik, A. Belyanin, and H. Munekata, Phys. Rev. B **83**, 125206 (2011).
15. Z. E. Kun'kova, E. A. Gan'shina, L. L. Golik, Yu. A. Danilov, A. V. Kudrin, V. I. Kovalev, G. S. Zykov, Yu. V. Markin, O. V. Vikhrova, and B. N. Zvonkov, Phys. Solid State **60**, 943 (2018).
16. Ye Yuan, Chi Xu, R. Hübner, R. Jakiela, R. Böttger, M. Helm, M. Sawicki, T. Dietl, and S. Zhou, Phys. Rev. Mater. **1**, 054401 (2017).
17. E. A. Gan'shina, L. L. Golik, Z. E. Kun'kova, G. S. Zykov, I. V. Bykov, A. I. Rukovishnikov, Ye Yuan, R. Böttger, and S. Zhou, J. Magn. Magn. Mater. **459**, 141 (2018).
18. D. Bürger, S. Zhou, M. Pandey, Ch. S. Viswanadham, J. Grenzer, O. Roshchupkina, W. Anwand, H. Reuther, V. Gottschalch, M. Helm, and H. Schmidt, Phys. Rev. B **81**, 115202 (2010).
19. S. Zhou, J. Phys. D **48**, 263001 (2015).
20. E. A. Balykina, E. A. Gan'shina, and G. S. Krinchik, Sov. Phys. JETP **66**, 1073 (1987).
21. P. Lautenschlager, M. Garriga, S. Logothetidis, and M. Cardona, Phys. Rev. B **35**, 9174 (1987).
22. H. Tanaka, W. M. Jadwisienczak, H. Saito, V. Zayets, S. Yuasa, and K. Ando, J. Phys. D **47**, 355001 (2014).
23. J. Szczytko, W. Bardyszewski, and A. Twardowski, Phys. Rev. B **64**, 075306 (2001).
24. T. Jungwirth, P. Horodyská, N. Tesařová, P. Němec, J. Šubrt, P. Malý, P. Kužel, C. Kadlec, J. Mašek, I. Němec, M. Orlita, V. Novák, K. Olejník, Z. Šobáň, P. Vašek, P. Svoboda, and J. Sinova, Phys. Rev. Lett. **105**, 227201 (2010).

Translated by A. Ivanov